CROATICA CHEMICA ACTA CCACAA **75** (1) 89–106 (2002)

ISSN-0011-1643
CCA-2784 *Original Scientific Paper*

Precipitation Diagrams of Struvite and Dissolution Kinetics of Different Struvite Morphologies

*Vesna Babić-Ivančić, Jasminka Kontrec, Damir Kralj, and Ljerka Brečević**

Laboratory for Precipitation Processes, Division of Materials Chemistry, Ruđer Bošković Institute, P. O. Box 180, HR-10002 Zagreb, Croatia

Received August 1, 2001; revised November 27, 2001; accepted November 27, 2001

Spontaneous precipitation in the systems $MgCl_2$–H_3PO_4–NH_4OH–NaCl (0.15 mol dm^{-3})–H_2O, $MgSO_4$–$NH_4H_2PO_4$–H_2O and $MgSO_4$–$NH_4H_2PO_4$–NaCl (0.15 mol dm^{-3})–H_2O was studied at 25 and 37 °C and initial pH = 4. Precipitates aged for 24 hours and 30 days were characterized by means of chemical analyses, X-ray diffractometry, FT-IR spectroscopy and thermogravimetry. Struvite was found to be the predominant phase formed in a wide range of reactant concentrations. The thermodynamic solubility products of struvite, $K_s^o = c(Mg^{2+}) \cdot \gamma_2 \cdot c(NH_4^+) \cdot \gamma_1 \cdot c(PO_4^{3-}) \cdot \gamma_3$, ($pK_s^o = 13.359 \pm 0.284$ at 25 °C and $pK_s^o = 13.269 \pm 0.113$ at 37 °C) were calculated from the final, equilibrium, pH values taking all the relevant magnesium, phosphate and ammonium species into account. The dissolution kinetics of dendrites and rod-like crystals of struvite in water was followed by recording pH as a function of time and the linear dependence of the dissolution rate on the absolute undersaturation was found. The dissolution rate constants k_{diss} were found to be 0.075, 0.103 and 0.152 $dm^3\ mol^{-2/3}\ s^{-1}$ for rod-like crystals, and 0.331, 0.286 and 0.596 $dm^3\ mol^{-2/3}\ s^{-1}$ for dendrites at 25, 30 and 37 °C, respectively. The activation energy for the dissolution of rod-like crystals was found to be (44.8 ± 1.1) kJ mol^{-1} and that for dendrites (37.6 ± 1.6) kJ mol^{-1}. Analysis of the kinetic data suggests the diffusion of constituting ions away from the surface of the dissolving crystal or the desorption of ions from the crystal adsorption layer as the possible rate determining mechanisms of struvite dissolution.

Key words: struvite, precipitation, thermodynamic solubility product, dissolution kinetics.

* Author to whom correspondence should be addressed. (E-mail: brecevic@rudjer.irb.hr)

INTRODUCTION

A distinctive characteristic of biological systems is the complexity of their chemical structure, *i.e.*, involvement of a great number of different chemical substances. The most important and certainly irreplaceable component for all living cells is water. Intracellular and extracellular fluids contain a variety of inorganic ions, among which Na^+, K^+, Ca^{2+}, Mg^{2+}, Cl^-, HPO_4^{2-}, HCO_3^- and SO_4^{2-} are the most abundant. These cations are essential for the growth and normal function of all living creatures. In the human body, these cations make up about 99% of the total metal ion contents.[1] Ca^{2+} and Mg^{2+} are constitutive elements of the development of structures such as bones, teeth and shells, in which these cations are mostly associated with phosphate and carbonate ions. However, if deposition occurs in a wrong place, it can result in stone formation, arterial disorders, *etc.*

Various phosphates are found in urinary stones. Most of them are calcium salts. Among magnesium phosphates, magnesium ammonium phosphate hexahydrate ($MgNH_4PO_4 \cdot 6H_2O$), commonly known as struvite, is of great practical relevance. Apart from being a frequent constituent of renal and vesicle calculi, especially those related to urinary tract infections,[2] this compound also appears naturally as a mineral and often occurs in scale deposits in the wastewater treatment industry.[3]

Due to its importance in many fields, struvite has been studied from different points of view and its chemical and physical properties have been described. Many interesting data are available concerning factors involved in stone formation,[4–7] application of struvite precipitation in the phosphorus recovery process in wastewater treatment systems,[8,9] as well as its occurrence in geological deposits.[10,11] Precipitation of struvite has been studied with regard to solution composition and pH,[12,13] and attention has been also paid to the kinetics and mechanism of struvite precipitation in the conditions of constant supersaturation.[14]

Nevertheless, for a better understanding of stone formation and its possible prevention, a more systematic physical chemical study of struvite is needed. In order to contribute to the knowledge of struvite, we have studied the influence of the initial reactant concentrations, ageing time and temperature on the composition and morphology of precipitates in the complex systems: $MgCl_2$–H_3PO_4–NH_4OH–NaCl (0.15 mol dm^{-3})–H_2O, $MgSO_4$–$NH_4H_2PO_4$–H_2O and $MgSO_4$–$NH_4H_2PO_4$–NaCl (0.15 mol dm^{-3})–H_2O. Special attention was paid to the investigating the possible difference in the solubility and dissolution kinetics of different struvite morphologies.

EXPERIMENTAL

All chemicals used were analytically pure, and the water was of high quality (conductivity < 0.1 μS cm^{-1}). Standardization of stock solutions was performed using classical analytical methods,[15] *i.e.*, magnesium was determined by complexometric titration, phosphate spectrophotometrically as the molybdenvanadato complex, phosphoric acid solution by titration with standard sodium hydroxide solution, sodium chloride by titration with standard silver nitrate solution, and ammonium hydroxide solution by titration with standard hydrochloric acid solution and also by using ammonium selective electrode (F2322NH_4) coupled with a calomel electrode (K701), connected to a pH meter (all Radiometer).

Precipitation systems were prepared by mixing equal volumes of previously thermostated magnesium chloride, or magnesium sulphate, solutions of known concentrations with phosphoric acid, or ammonium dihydrogenphosphate, solutions pre-adjusted to pH = 7.4 by adding required amounts of ammonium hydroxide. If not otherwise stated, the latter solutions also contained 0.3 mol dm^{-3} NaCl. After initial mixing of reactant solutions, the system was tightly closed, leaving a minimum space above the solution and no other agitation was employed. All experiments were performed at 25 and 37 °C and the precipitation systems were aged for 24 hours and 30 days. After these periods of time, the morphology of the precipitate was observed by optical microscopy (Orthoplan photographic microscope, E. Leitz, Wetzlar). The pH of the systems was measured by means of a combined glass-calomel electrode (GK 2401 C) connected to a pH meter and standardized by a series of buffers 4.005 < pH < 10.01 (all Radiometer). Selected samples were prepared in large amounts, the suspensions were filtered through a 0.45 μm membrane filter, and the precipitates were washed with small portions of water and dried at room temperature. The composition of the precipitates was identified by X-ray diffractometry, XRD (Philips counter diffractometer with graphite monochromatized Cu-Kα radiation), Fourier transform infrared, FT-IR, spectroscopy (Mattson FT-IR spectrophotometer, Genesis Ser.) and thermogravimetry, TGA (Mettler TG 50 thermo balance with TC 11 TA processor). The specific surface area, SSA, was determined by the B.E.T. method using nitrogen (Flow SorbII 2300, Micromeritics). For chemical analysis of supernatants, phosphate was determined spectrophotometrically, magnesium by retitration of the excess of Na_2EDTA with $MgCl_2$ standard solution,[15] and ammonium using an ammonium selective electrode.

Dissolution experiments were performed in a thermostated reaction vessel, in which the known amount of dry precipitate was suspended in 130.0 cm^3 water. Immediately after suspending the crystals, the reaction vessel was tightly closed, leaving no space for air inside the vessel, thus preventing any further exchange of carbon dioxide and ammonium between the system and the air. These experiments were carried out at (25.0 ± 0.1) °C, (30.0 ± 0.1) °C and (37.0 ± 0.1) °C. During the experiment, the system was continuously stirred at a constant rate by means of a Teflon-coated magnetic stirring bar. The progress of the reaction was followed by monitoring pH as a function of time by means of a combined glass-calomel electrode (GK 2401 C) connected to a digital pH meter (ION 85, Radiometer) and a computer (SHARP – PC 6200). Commercial standard buffer solutions (Radiometer) were used to adjust the instrument (pH = 7.00 and 10.01 at 25 °C) before the experiment started. At the end of each experiment, the remaining solid phase was analysed by FT-IR

spectroscopy and the supernatant was analysed for magnesium using the above-mentioned method of retitration.

Treatment of Data

The best estimates of the thermodynamic solubility products of struvite, $K_s^o = c(Mg^{2+}) \cdot \gamma_2 \cdot c(NH_4^+) \cdot \gamma_1 \cdot c(PO_4^{3-}) \cdot \gamma_3$, were made from the total initial molar concentrations of $MgSO_4$, $NH_4H_2PO_4$, NaCl and NH_4OH, the measured equilibrium pH and the total molar concentration of magnesium. In the calculations, the chemical equilibrium of 17 ionic species, the mass balance equations for total magnesium (Mg_{tot}), phosphate (P_{tot}), sodium (Na_{tot}), ammonium (A_{tot}), and sulphate (S_{tot}), as well as the charge balance equation were taken into account. The respective chemical equilibria and the corresponding stability constants are listed in Table I. It should be emphasized that the equilibrium constant for the formation of $NaHPO_4^-$ was found only for 25 °C. Therefore, the same value,[16] $\log k_{Na}^o = 0.85$, was used for all temperatures.

The activity coefficients, γ_z, were obtained from the modification of the Debye-Hückel equation proposed by Davies[18]

$$\log \gamma_z = -Az_i^2 \left[\frac{(I / \text{mol dm}^{-3})^{1/2}}{1 + (I / \text{mol dm}^{-3})^{1/2}} - 0.3(I / \text{mol dm}^{-3}) \right] \quad (1)$$

where A is the Debye-Hückel constant dependent on temperature,[19] z_i is the charge of an ion and I is the ionic strength, defined by

$$I = \frac{1}{2} \sum_i c_i z_i^2 \quad (2)$$

with c_i being the molar concentration.

Equation (1) gives a reasonable estimate of the activity coefficients at the ionic strengths up to 0.5 mol dm^{-3}, as in the present study.

The molar concentration of chloride ions was taken to be identical to the initial concentration of sodium chloride added to the system in order to maintain the ionic strength.

The dissolution rates were calculated by means of both the initial total mass of struvite (either dendrites or rod-like crystals) and the amount of crystals dissolved at time t. The amount of struvite dissolved at any moment of the dissolution process was calculated from the recorded pH, defined by $pH = -\log([H^+] \gamma_1)$, the known initial concentration* of CO_2 dissolved,[20] and taking the following ionic species into account: H^+, OH^-, $H_2PO_4^-$, HPO_4^{2-}, PO_4^{3-}, $MgPO_4^-$, $MgHPO_4^o$, Mg^{2+}, NH_4^+, $NH_3(aq)$, HCO_3^-, CO_3^{2-}. In addition to the equilibrium relations listed in Table I, the charge and the mass balance equations for total concentrations of carbonate (C_{tot}), phosphate (P_{tot1}),

---

* Carbon dioxide is present in a reactant aqueous solution as a contaminant before the dissolution experiments start. Its complete removal from the solution is difficult, as well as the protection of solution from subsequent recontamination. Therefore, the examined system was closed to the atmosphere and the amount of carbon dioxide dissolved was calculated from the pH of pure water determined before each experiment started.

and magnesium (Mg_{tot1}), as well as the relation describing the equilibrium between carbonate and bicarbonate ions were also taken into account.[21]

Subtracting the amount of struvite dissolved from the initial amount of crystals added, the amount still undissolved was found. The number and the shape of the crystals were assumed to be constant during the dissolution kinetics. The dissolution rate, dc/dt, was determined by numerical differentiation of the concentration of the struvite dissolved, as a function of time. Driving force for the dissolution process, given as an absolute undersaturation, $c_s - c$, was calculated by subtracting the concentration of the struvite dissolved from the solubility, c_s.

The struvite dissolution, under the given experimental conditions, was found to follow the kinetic equation

$$dc/dt = k_d \cdot \frac{A}{V} \cdot (c_s - c) \tag{3}$$

where A is the surface area of the suspended crystals and V is the volume of liquid. This equation was adapted for evaluation of the experimental data. Thus, A was expressed as a function of the number of crystals, N, and the amount of struvite in the crystal phase suspended in the solution, n_s, *i.e.*, $A = N f_A \cdot l^2$; $V_m n_s = N f_V \cdot l^3$; where f_A and f_V are the dimensionless numerical surface and volume factors dependent on the shape, V_m is the molar volume of struvite and l is the linear dimension of suspended crystals.

$$dc/dt = k_d \cdot f_A \cdot f_V^{-2/3} \cdot V_m^{2/3} \cdot N^{1/3} \cdot \frac{n_s^{2/3}}{V} \cdot (c_s - c) \tag{4}$$

Equation (4) can also be expressed as:

$$dc/dt = k_{diss} \cdot \frac{n_s^{2/3}}{V} \cdot (c_s - c) \tag{4a}$$

In the above expressions, k_d and k_{diss} are the dissolution rate constants.

The differential equation, Eq. (4a), was used in setting the mathematical model of struvite dissolution. For this purpose, the equation was solved numerically using the experimentally determined constants and the following initial conditions: $c_o = 0$ mol dm^{-3} , $t_o = 0$ s. The solubility and the initial amount of crystal seeds corresponded to the experimental conditions applied.

RESULTS AND DISCUSSION

Figure 1 shows concentration diagrams of magnesium phosphates in the system $MgSO_4$–$NH_4H_2PO_4$–NaCl (0.15 mol dm^{-3})–H_2O at 25 °C (Figure 1a) and 37 °C (Figure 1b). Both diagrams represent the system aged for 30 days, the time that was found to be long enough to establish equilibrium between the solid phase and its supernatant. Precipitation boundaries (between clear solutions and the first detectable precipitate) and region boundaries (separate regions of precipitates with different morphology) are denoted by thick and thin solid lines, respectively. Thick dashed lines in both

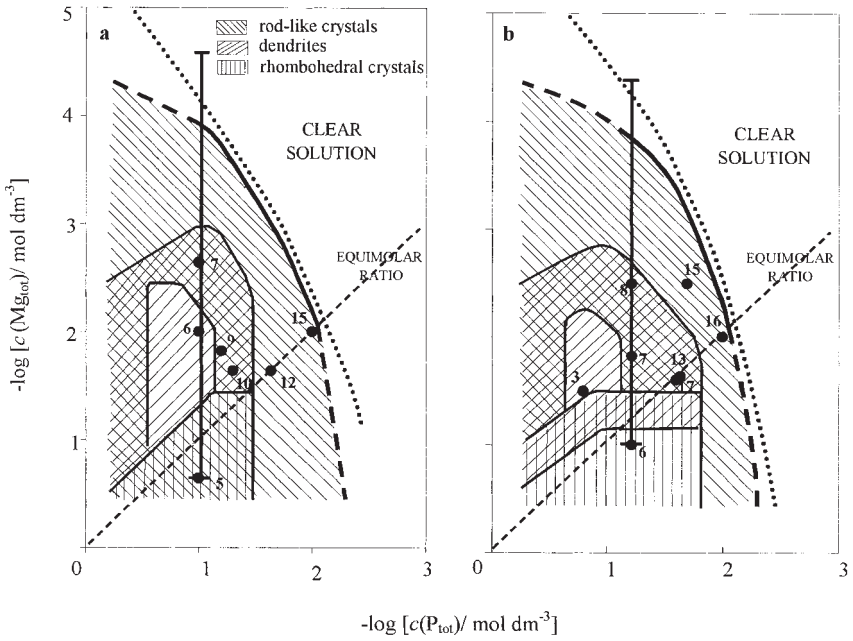

Figure 1. Concentration diagrams with assigned precipitation (thick solid lines) and region boundaries (thin solid lines) of the system $MgSO_4$–$NH_4H_2PO_4$–NaCl (0.15 mol dm^{-3})–H_2O, pH_i = 7.4, aging time 30 days, 25 °C (a) and 37 °C (b). Thick dashed lines mark the uncertain parts of precipitation boundaries. The positions of the solubility boundaries (thick dotted lines), were calculated from the data listed in Table I. Hatched areas indicate the regions within which precipitates of similar morphology are formed. Solid circles denote samples selected for detailed analyses. Cross-sections correspond to the precipitation curves shown in Figure 2.

diagrams mark the parts of the precipitation boundary in which distinction between the clear solution and the precipitate was not entirely certain. Positions of the solubility boundaries, calculated from the data listed in Table I and the thermodynamic solubility products obtained in this work, are denoted by thick dotted lines. Hatched areas illustrate the concentration regions within which precipitates of similar morphology were formed. Cross-hatched areas denote the concentration regions within which two different morphologies were observed. Samples selected for detailed chemical and structural analyses, prepared in large amounts, are assigned by solid circles and numbered.

The other two precipitation systems studied in this work, $MgSO_4$–$NH_4H_2PO_4$–H_2O and $MgCl_2$–H_3PO_4–NH_4OH–NaCl (0.15 mol dm^{-3})–H_2O, both at 25 °C and 37 °C, show no differences in the boundary positions and morphology of the precipitates from the above system represented.

TABLE I

Equilibrium constants (I = 0) used in calculations

Equilibrium	Constant	log K^o (37 °C)	log K^o (25 °C)	Ref.
$H_2PO_4^- + H^+ \leftrightarrow H_3PO_4^0$	K_1	2.21	2.148	16
$HPO_4^{2-} + H^+ \leftrightarrow H_2PO_4^-$	K_2	7.18	7.198	16
$PO_4^{3-} + H^+ \leftrightarrow HPO_4^{2-}$	K_3	12.18	12.375	16
$HPO_4^{2-} + Na^+ \leftrightarrow NaHPO_4^-$	K_{Na}	0.85	0.85	16
$H_2PO_4^- + Mg^{2+} \leftrightarrow MgH_2PO_4^+$	K_{Mg}	1.207	1.207	17
$HPO_4^{2-} + Mg^{2+} \leftrightarrow MgHPO_4^0$	K_{Mg1}	2.815	2.428	17
$PO_4^{3-} + Mg^{2+} \leftrightarrow MgPO_4^-$	K_{Mg2}	4.92	4.92	17
$SO_4^{2-} + H^+ \leftrightarrow HSO_4^-$	K_4	2.03	1.99	16
$SO_4^{2-} + Mg^{2+} \leftrightarrow MgSO_4^0$	K_{Mg3}	1.97	2.23	16
$NH_4^+ \leftrightarrow NH_3(aq) + H^+$	K_5	9.25	9.24	14
$H_2O \leftrightarrow H^+ + OH^-$	K_w	–13.62	–13.997	16

Each of the precipitation diagrams has been constructed from a series of precipitation curves, such as shown in Figure 2. The two curves represented are denoted as cross-sections in Figures 1a and 1b. These precipitation cur-

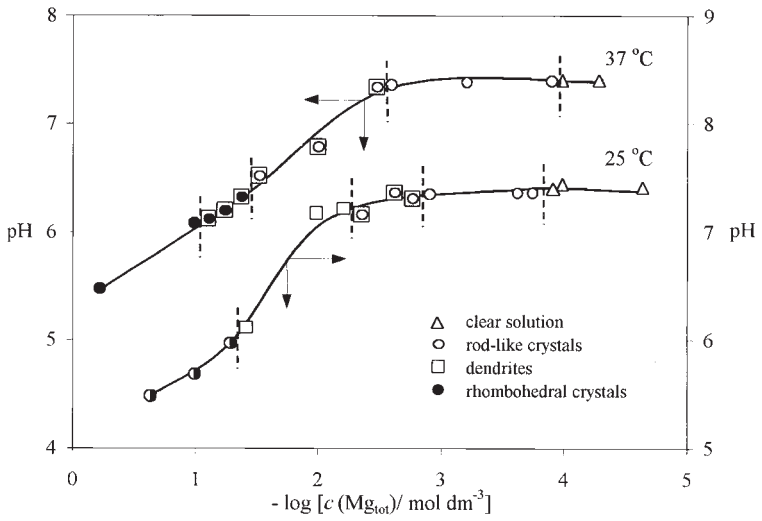

Figure 2. Precipitation curves, pH *versus* $c(Mg_{tot})$, correspond to the cross-sections in Figures 1a (25 °C) and 1b (37 °C). Initial reactant concentrations: $c(P_{tot}) = 1 \times 10^{-1}$ mol dm^{-3} , $c(A_{tot}) = 1.96 \times 10^{-1}$ mol dm^{-3} at 25 °C; $c(P_{tot}) = 6 \times 10^{-2}$ mol dm^{-3}, $c(A_{tot}) = 1.12 \times 10^{-1}$ mol dm^{-3} at 37 °C; c(NaCl) = 0.15 mol dm^{-3}, aging time 30 days. Dashed lines correspond to the precipitation and region boundaries in Figure 1.

ves are plots of the final pH values of supernatants against the initial concentration of total magnesium at constant concentrations of total phosphate (1.00×10^{-1} mol dm^{-3} at 25 °C, 6.0×10^{-2} mol dm^{-3} at 37 °C) and total ammonium (1.96×10^{-1} mol dm^{-3} at 25 °C, 1.12×10^{-1} mol dm^{-3} at 37 °C). The morphological types of precipitates, isolated 30 days after sample preparation, are indicated by different designations.

Micrographs of the typical morphology of the precipitates are shown in Figure 3. According to the three methods used to characterize the precipitates, the forms of crystals demonstrated in Figures 3a and 3b were found to be characteristic of struvite and the form shown in Figure 3c to be charac-

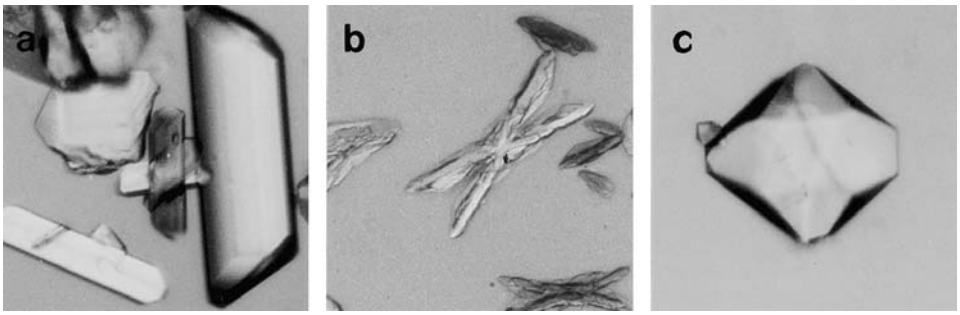

Figure 3. Micrographs showing the typical morphology of precipitates: (a) rod-like crystals, (b) dendritic crystals, (c) rhombohedral crystals. Magnification 150 ×.

teristic of magnesium hydrogen phosphate trihydrate ($MgHPO_4 \cdot 3H_2O$), known as newberyite. As an example, X-ray diffraction patterns, FT-IR spectra and thermograms of samples 3, 6 and 15, displayed in Figure 1b, are shown in Figure 4. Samples 3 and 15, which precipitated in the form of dendrites (Figure 3b) and rod-like crystals (Figure 3a) respectively, exhibit identical XRD patterns (Figures $4a_1$ and a_2) and FT-IR spectra (Figures $4b_1$ and b_2), both characteristic of struvite.[22–24] Thermogravimetric analyses (Figures $4c_1$ and c_2) show that a weight loss of both samples started at about 60 °C and continued until about 400 °C, when all of the water and ammonium was released. The peak temperature is found to be about 113 °C for dendrites and about 118 °C for rod-like crystals at the heating rate of 20 °C min^{-1}. The weight loss per struvite molecule, including all the analysed samples, amounted to $w = (50.82 \pm 0.16)\%$ (the theoretical value is $w = 51.37\%$). Sample 6 precipitated in the form of rhombohedral crystals (Figure 3c). Its XRD pattern (Figure $4a_3$) and FT-IR spectrum (Figure $4b_3$) are characteristic of newberyite.[22–24] TGA (Figure $4c_3$) shows that the loss of water started at about 100 °C and continued to about 500 °C, when nearly all wa-

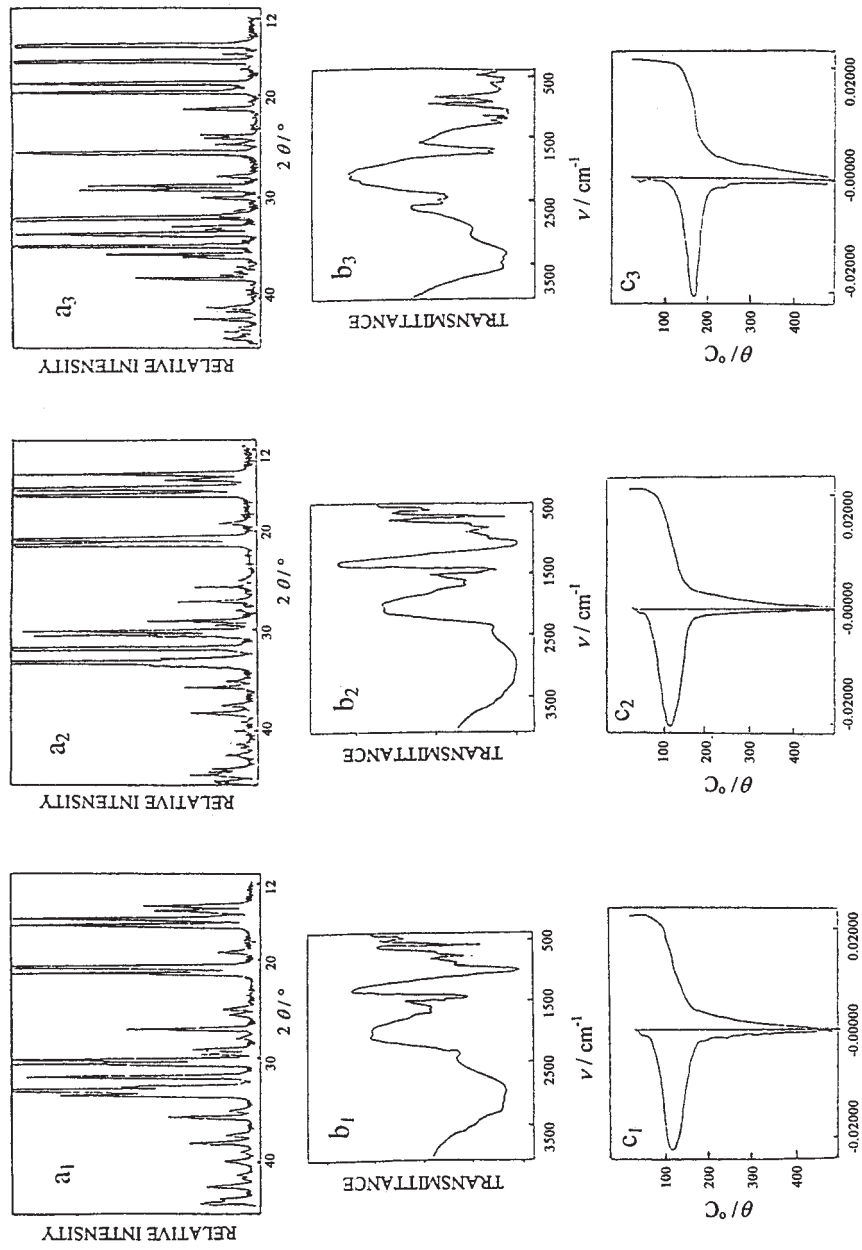

Figure 4. X-ray diffraction patterns, FT-IR spectra and thermograms of samples 3, 6 and 15, shown in Figure 1b.

ter was released. The peak temperature is about 167 °C at the heating rate of 20 °C min^{-1}. The total loss of weight up to 500 °C corresponds to about 3.1 molecules of water per molecule of newberyite.

It is interesting to note that the morphology and the composition of precipitates depend on the initial reactant concentrations and on temperature. A comparison of Figures 1a and 1b shows that the concentration region within which dendritic crystals of struvite appear, taking together regions of pure dendrites and dendrites in a mixture with a different morphology, is larger at 37 °C than at 25 °C. At 25 °C, however, a larger concentration region exists in which only dendritic crystals precipitate. It is also obvious that the region in which newberyite crystallizes is larger at 37 °C than at 25 °C and that the region of pure newberyite appears at 37 °C only. These observations are in accordance with some previous findings,[12] according to which newberyite is a stable form at high concentrations of magnesium and at a low pH (see Figure 2). Struvite, which seems to nucleate first in this concentration region, evidently transforms much faster into newberyite at higher temperature.[12]

Samples at equimolar concentrations of magnesium and phosphate (Figures 1a and 1b, samples 12 and 15 at 25 °C, samples 13, 16 and 17 at 37 °C) and some not far from their equimolar ratio (samples 9 and 10 at 25 °C and sample 7 at 37 °C) were chosen for the determination of struvite solubility. Each of these samples was prepared several times and analysed. The initial reactant concentrations and the mean values of the magnesium equilibrium concentrations used in computation are summarized in Table II. From the

TABLE II

Initial (i) total concentrations of magnesium (Mg_{tot}), phosphate (P_{tot}), ammonium (A_{tot}), and equilibrium (eq) total concentrations of magnesium and pH, used in the calculations of K_s^o; c(NaCl) = 0.15 mol dm^{-3}, pH_i = 7.40, aging time is 30 days

Sample	$\frac{\theta}{°C}$	$\frac{10^2\, c_i(Mg_{tot})}{mol\ dm^{-3}}$	$\frac{10^2\, c_i(P_{tot})}{mol\ dm^{-3}}$	$\frac{10^2\, c_i(A_{tot})}{mol\ dm^{-3}}$	$\frac{10^2\, c_{eq}(Mg_{tot})}{mol\ dm^{-3}}$	pH_{eq}
9	25	1.5	6.0	11.20	0.057	6.59
10	25	2.3	5.0	10.20	0.381	6.45
12	25	2.3	2.3	4.25	1.542	6.14
15	25	1.0	1.0	1.93	0.707	6.55
17	37	2.5	2.5	4.94	1.510	6.09
13	37	2.3	2.3	4.25	1.600	6.16
7	37	1.5	6.0	11.20	0.054	6.56
16	37	1.0	1.0	1.93	0.746	6.61

solubility data, the standard equilibrium solubility constants of struvite were estimated. The calculated values were found to be $pK_s^o = 13.359 \pm 0.284$ at 25 °C and $pK_s^o = 13.269 \pm 0.113$ at 37 °C. These are in good agreement with the values reported in literature.[3,25]

In the pH region $5 < pH < 7.4$, $H_2PO_4^-$ and HPO_4^{2-} are the prevalent phosphate species in solution. According to the following reaction

$$Mg^{2+} + NH_4^+ + H_2PO_4^- + 6H_2O \rightleftharpoons 2H^+ + MgNH_4PO_4 \cdot 6H_2O\ (s) \qquad (5)$$

a change in the pH, owing to precipitate formation or dissolution, is expected. The amount of liberated/bound H^+ ions depends on the amount and composition of the solid phase precipitated/dissolved. Therefore, pH was used as a measure of the dissolution process progress.

The dissolution experiments of two morphological modifications of struvite, dendritic and rod-like crystals (samples 3 and 15, respectively, denoted in Figure 1b), were performed at 25, 30 and 37 °C. The specific surface area of these crystals was found to be (0.22 ± 0.05) $m^2\ g^{-1}$ and (0.09 ± 0.03) $m^2\ g^{-1}$, respectively. At each temperature, different amounts of a particular struvite modification were dissolved. Figure 5 shows the curves, pH as a function of time, obtained at 25 °C by stirring different amounts of the dendritic seed crystals of struvite with water. The pH measured during the process increased gradually until it became constant. In the cases when the amount of struvite was larger than that which can be dissolved, the maximum, equilibrium, pH was found to be between 9.60 and 9.75. Thus obtained values are lower than the equilibrium value ($pH_{sat} = 9.842$) calculated on the basis of K_s^o, determined in this paper. The difference results from the amount of carbon dioxide dissolved in water. The initial pH of water used in the experiments varied from $pH_i = 5.3$ to $pH_i = 5.8$. Table III shows how the solubility of struvite and pH of the saturated solution of struvite depend on the different amounts of CO_2 dissolved in pure water. Although the solubility of struvite is not much affected, the final pH significantly changes in the presence of carbon dioxide.

The plots of total concentrations of struvite in solution during dissolution of different amounts of dendritic crystals are shown in Figure 6. These concentrations were calculated from the pH values of the corresponding curves shown in Figure 5. The dashed line indicates the value that refers to the solubility calculated for struvite dendrites dissolved in water having $pH_i = 5.5$ (see Table III). The smooth curves, representing the model curves, fit well the experimental curves, except in their initial part. This is mainly due to the fast rate of the dissolution process in its initial part and a relative slowness in the electrode response. In the experiment in which the largest amount of struvite was added, 408.5 mg dm^{-3}, the equilibrium was estab-

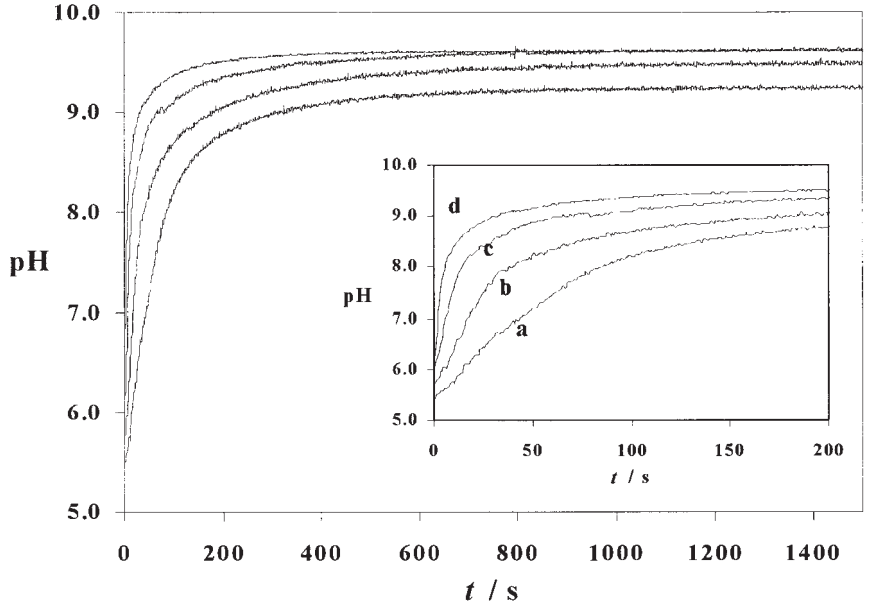

Figure 5. pH as a function of time during dissolution of different initial amounts of dendritic crystals of struvite at 25 °C: (a) 40.8 mg dm^{-3}, (b) 82.3 mg dm^{-3}, (c) 157.7 mg dm^{-3} and (d) 408.5 mg dm^{-3}.

lished relatively fast, after approximately 1200 seconds, and a certain amount of struvite remained still undissolved. The amounts of struvite of 82.3 and 40.8 mg dm^{-3} were less than the amount that can be dissolved at 25 °C.

In order to find out the mechanism of the dissolution process, different theoretical models were tested. The plots according to Eq. (3) gave straight lines. In that case, the value of A was taken to be the initial surface area of

TABLE III

Total concentration of CO_2 dissolved in water $c_{tot}(CO_2)$, solubility of struvite (c_s), and pH of saturated solution (pH_{sat}), at the initial pH of water contaminated with CO_2

pH_i	$c_{tot}(CO_2)$ / mol dm^{-3}	c_s / mol dm^{-3}	pH_{sat}
7.00	–	5.258×10^{-4}	9.842
5.50	2.6×10^{-5}	5.300×10^{-4}	9.771
5.30	6.2×10^{-5}	5.380×10^{-4}	9.676
5.20	9.6×10^{-5}	5.477×10^{-4}	9.590

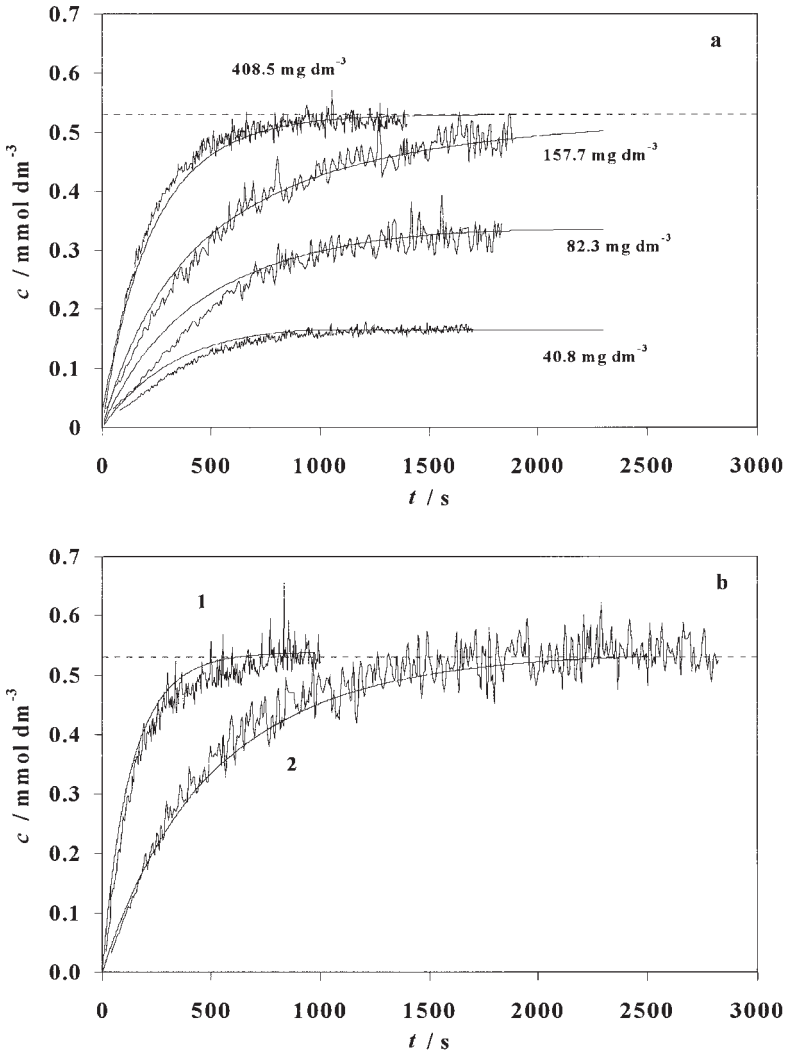

Figure 6. Plots of the total concentration of struvite in solution as a function of time during dissolution of (a) different amounts of dendritic crystals of struvite at 25 °C, and (b) 400.0 mg dendritic (1) and 400.8 mg rod-like crystals (2) at 30 °C. The curves were calculated from the variation of pH with time, as shown in Figure 5. Smooth lines correspond to the model curves.

the crystals dissolved. Since f_A was unknown, it was not possible to evaluate the change of A during the dissolution process. This primarily refers to dendrites. The dissolution constant, k_d, thus obtained for the dissolution of dendrites was 2 to 3 times higher than that for rod-like crystals. Therefore, the

dissolution rates, dc/dt, calculated from the concentration *versus* time dependence, were plotted as a function of the product of absolute undersaturation, $c_s - c$, and the amount of struvite present in suspension at the given time, $n_s^{2/3}$. In this way, a correction for the constant calculation was implemented and the validity of the kinetic model, given by Eq. (4a), was tested. Figure 7 shows these plots for the dissolution of dendritic and rod-like crystals of struvite at 25 °C. From the slopes of these straight lines, the values of rate constants, k_{diss}, for the dissolution processes were calculated. The results are given in Table IV. In spite of the correction applied, the mean values of the dissolution rate constants of dendrites are still 3.9, 4.0 and 4.4 times higher than the respective values of the rod-like crystals at the same temperatures. The difference in shapes between the two morphologies, *i.e.*, the difference in f_A and f_V from Eq. (4), seems to be the only possible explanation of the difference in the dissolution rate constants obtained.

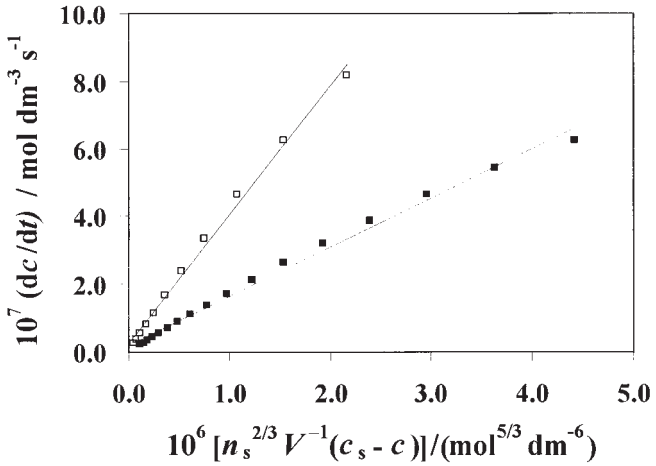

Figure 7. Plots of dc/dt as a function of $n_s^{2/3}V^{-1}(c_s - c)$ for dissolution kinetics of dendritic (open squares) and rod-like (full squares) crystals of struvite at 25 °C. From the slopes of the straight lines, the dissolution rate constants, k_{diss}, were calculated. The initial mass concentration of dendritic crystals was 408.5 mg dm^{-3} and that of rod-like crystals was 409.2 mg dm^{-3}.

These mean values of dissolution rate constants, calculated for each of the three temperatures applied, and for the two morphologies of seed crystals, were used in setting the mathematical model of struvite dissolution. An example of the model curves is shown in Figure 6 (smooth curves superimposed on the experimental curves). These curves fit satisfactorily well the

TABLE IV

Dissolution rate constants, k_{diss}, of different struvite morphologies, calculated from the dissolution kinetics and the mean values of these constants at each of the applied temperatures. The experiments were initiated by introducing different initial masses of seed crystals, ρ_s

θ / °C	Dendritic crystals			Rod-like crystals		
	ρ_s / g dm^{-3}	k_{diss} / dm^3 mol$^{-2/3}$ s^{-1}	$< k_{diss} >$ / dm^3 mol$^{-2/3}$ s^{-1}	ρ_s / g dm^{-3}	k_{diss} / dm^3 mol$^{-2/3}$ s^{-1}	$< k_{diss} >$ / dm^3 mol$^{-2/3}$ s^{-1}
25.0	408.5	0.347	0.331 ± 0.030	410.8	0.074	0.076 ± 0.017
	157.7	0.317		409.2	0.060	
	82.3	0.364		156.2	0.099	
	40.8	0.298		81.5	0.067	
30.0	396.2	0.397	0.416 ± 0.024	770.8	0.114	0.103 ± 0.014
	166.9	0.427		390.8	0.093	
	81.5	0.444		161.5	0.119	
	42.3	0.394		80.8	0.102	
				42.3	0.087	
37.0	777.7	0.604	0.596 ± 0.073	790.8	0.171	0.152 ± 0.017
	400.0	0.501		400.8	0.160	
	168.5	0.678		170.0	0.145	
	40.0	0.600		41.5	0.132	

experimental curves, which proves that the kinetics of struvite dissolution is well described by Eq. (4a). However, the dissolution process mechanism cannot be determined only by means of this kinetic model. The linear relation between the dissolution rate and undersaturation offers two possibilities for the rate determining step: diffusion of the constituting ions away from the crystal surface and the process at the crystal surface.[26,27] Since the typical values of the activation energies for these two processes differ significantly (usually E_a = 10 to 25 kJ mol^{-1} for the bulk diffusion and $E_a \approx$ 45 kJ mol^{-1} for the adsorption/desorption), the Arrhenius plot was made. The dissolution rate constants from Table IV are plotted in Figure 8 against the reciprocal of the absolute temperature in order to determine the activation energy for dissolution of dendritic and rod-like crystals of struvite. The straight lines best-fitted to the two sets of points are represented by

$$\ln (k_{diss} / \mathrm{dm^3\ mol^{-2/3}\ s^{-1}}) = 15.5 - (5390\ T^{-1}) / \mathrm{K^{-1}} \quad (6)$$

for the rod-like crystals, and by

$$\ln (k_{\text{diss}} / \text{dm}^3\ \text{mol}^{-2/3}\ \text{s}^{-1}) = 14.1 - (4525\ T^{-1}) / \text{K}^{-1} \quad (7)$$

for dendrites.

From the slopes of these lines, the activation energies, $E_a = (44.8 \pm 1.1)$ kJ mol^{-1} and $E_a = (37.6 \pm 1.6)$ kJ mol^{-1}, for dissolution of rod-like and dendritic crystals of struvite, respectively, were calculated. These two relatively similar values indicate that the rate determining mechanism of dissolution in both cases could be the same. According to the activation energies obtained, the most probable rate determining mechanism is the process of desorption of the integrating ions. Nevertheless, few arguments are in favour of the diffusion-controlled mechanism. The first of them is empirical: there are many examples[26] in which dissolution of electrolytes, even of those that grow by a surface mechanism, is controlled by diffusion. The second argument in favour of diffusion-controlled dissolution is the fact that the value of k_{diss} obtained for dendrites is higher than k_{diss} for the rod-like crystals. This is expected if one knows that dendritic crystals have many more corners and edges than the compact morphological forms. The stagnant diffusion layer is much thinner at the corners and edges, so that, if diffusion is the rate-determining step, the overall dissolution process is faster. In addition to the pre-

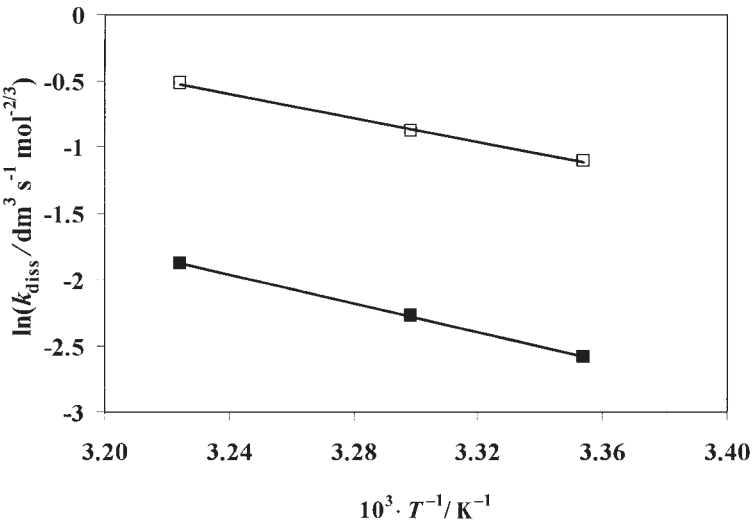

Figure 8. Arrhenius plot, ln k_{diss}, as a function of the reciprocal of the absolute temperature for dissolution of dendritic (open squares) and rod-like (full squares) crystals of struvite.

viously mentioned assumptions of the possible mechanisms of struvite dissolution, there is also a third one – the interplay of at least two rate controlling mechanisms. This possibility might even be the most realistic one, since it is based on the fact that the undersaturation range investigated in this work was quite large, so that the rate control may go from one mechanism to another upon a change of concentration.

REFERENCES

1. N. N. Hughes, *The Inorganic Chemistry of Biological Processes*, John Wiley & Sons Ltd., Chichester, 1985.
2. B. F. Schwartz, *Current Pharmaceutical Design* **5** (1999) 503–513.
3. K. N. Ohlinger, T. M. Young, and E. D. Schroeder, *Water Res.* **32** (1998) 3607–3614.
4. D. J. Sutor, *Brit. J. Urol*. **47** (1975) 585–587.
5. S. D. Roberts and M. I. Resnick, *Urinary stone matrix and urinary macromolecules*, in: P. O. Schwille, L. H. Smith, W. G. Robertson, and W. Vahlensieck (Eds.), *Urolithiasis and Related Clinical Research*, Plenum Press, New York, 1985, pp. 911–918.
6. J. Huhosson, L. Grenabo, H. Hedelin, S. Pettersson, and I. Tarfusser, *Urol. Res.* **18** (1990) 413–417.
7. A. Hesse and D. Heimbach, *World J. Urol.* **17** (1999) 308–315.
8. J. R. Buchanan, C. R. Mote, and R. B. Robinson, *Trans. ASAE* **37** (1994) 617–621; 1301–1308.
9. R. D. Schuiling and A. Andrade, *Environ. Technol.* **20** (1999) 765–768.
10. G. J. Handschuh and L. E. Orgel, *Science* **179** (1973) 483–484.
11. D. Mc Connell, *Science* **181** (1973) 582–582.
12. F. Abbona, H. E. Lundager Madsen, and R. Boistelle, *J. Crystal Growth* **57** (1982) 6–14; **74** (1986) 581–590; **89** (1988) 592–602.
13. F. Abbona and M. Franchini-Angela, *J. Cryst. Growth* **104** (1990) 661–671.
14. N. Ch. Bouropoulos and P. G. Koutsoukos, *J. Cryst. Growth* **213** (2000) 381–388.
15. A. Vogel, *A Textbook of Quantitative Inorganic Analysis Including Instrumental Analysis*, Longman, New York, 1978.
16. R. M. Smith and A. E. Martell, *Critical Stability Constants*, Vol. 6, Plenum Press, 1989.
17. C. W. Childs, *Inorg. Chem.* **9** (1970) 2465–2469.
18. C. W. Davies, *Ion Association*, Butterworths, London, 1962.
19. R. A. Robinson and R. H. Stokes, *Electrolyte Solutions*, 2nd edn., Butterworths, London, 1959.
20. D. Kralj, Lj. Brečević, and A. E. Nielsen, *J. Cryst. Growth* **143** (1994) 269–276.
21. D. Kralj and Lj. Brečević, *Colloids and Surfaces. A: Physicochem. Eng. Aspects* **96** (1995) 287–293.
22. Powder Diffraction File, Inorganic Card No. 15–762, 19–762, 19–762A, and 20–153, International Centre for Diffraction Data, Newtown Square, PA, USA.
23. A. Hesse and D. Bach, *Harnstein*, *Pathobiochemie und Klinisch-chemische Diagnostic*, in: H. Breuer, H. Büttner, and D. Stamm (Eds.), *Klinische Chemie in Einzeldarstellungen*, Georg Thieme, Stuttgart, 1982.

24. A. Hesse and G. Sanders, *Atlas of Infrared Spectra for the Analysis of Urinary Concrements*, Georg Thieme, Stuttgart, 1988.
25. E. V. Musvoto, M. C. Wentzel, and G. A. Ekama, *Water Res.* **34** (2000) 1868–1880.
26. Lj. Brečević and D. Kralj, *Kinetics and Mechanism of Crystal Growth in Aqueous Systems*, in: N. Kallay (Ed.), *Interfacial Dynamics*, Marcel Dekker, Inc., New York, Basel, 2000, pp. 435–474.
27. A. E. Nielsen, *Precipitates: Formation, Coprecipitation, and Aging*, in: I. M. Kolthoff and P. J. Elving (Eds.), *Treatise on Analytical Chemistry*, 2nd edn., Vol. 3, J. Wiley, New York, 1983, pp. 269–347.

SAŽETAK

Taložni dijagrami i kinetika otapanja različitih morfologija struvita

Vesna Babić-Ivančić, Jasminka Kontrec, Damir Kralj i Ljerka Brečević

Proučavano je spontano taloženje u sustavima $MgCl_2$–H_3PO_4–NH_4OH–NaCl (0.15 mol dm^{-3})–H_2O, $MgSO_4$–$NH_4H_2PO_4$–H_2O i $MgSO_4$–$NH_4H_2PO_4$–NaCl (0.15 mol dm^{-3})–H_2O pri temperaturama 25 i 37 °C, te početnom pH = 7,4. Talozi su stareni 24 sata i 30 dana i karakterizirani kemijskom analizom, röntgenskom difraktometrijom, FT-IR spektroskopijom i termogravimetrijom. Nađeno je, da se u širokom koncentracijskom području reaktanata taloži struvit. Termodinamičke ravnotežne konstante otapanja struvita, $K_s^o = c(Mg^{2+}) \cdot \gamma_2 \cdot c(NH_4^+) \cdot \gamma_1 \cdot c(PO_4^{3-}) \cdot \gamma_3$, ($pK_s^o$ = 13,359 ± 0,284 pri 25 °C i pK_s^o = 13,269 ± 0,113 pri 37 °C) izračunane su iz konačnih, ravnotežnih, vrijednosti pH, uzimajući u obzir sve relevantne magnezijeve, fosfatne i amonijeve ionske vrste. Kinetike otapanja dendritnih i štapićastih kristala struvita u vodi praćene su kao promjena pH s vremenom, te je nađena linearna ovisnost brzine otapanja o apsolutnoj podzasićenosti. Nađeno je, da konstante brzine otapanja k_{diss}, pri 25, 30 i 37 °C, iznose 0,075; 0,103 i 0,152 $dm^3\ mol^{-2/3}\ s^{-1}$ za štapićaste kristale, a 0,331; 0,286 i 0,596 $dm^3\ mol^{-2/3}\ s^{-1}$ za dendrite. Za energije aktivacije otapanja štapićastih kristala dobiven je iznos od (44,8 ± 1,1) kJ mol^{-1}, a dendrita (37,6 ± 1,6) kJ mol^{-1}. Analiza kinetičkih podataka upućuje na to, da je brzina otapanja struvita, pri danim eksperimentalnim uvjetima, kontrolirana ili difuzijom konstitucijskih iona s površine kristala u otopinu ili procesom desorpcije iona iz adsorpcijskog sloja kristala.